

# Subpolar activation of halogen heterogeneous chemistry in austral spring

Brian Zambri<sup>1</sup>, Douglas Edward Kinnison<sup>2</sup>, and Susan Solomon<sup>3</sup>

<sup>1</sup>Massachusetts Institute of Technology

<sup>2</sup>NCAR/CLAS

<sup>3</sup>MIT

November 26, 2022

## Abstract

Heterogeneous halogen chemistry plays a dominant role in driving changes in polar chemical composition and ozone depletion. Activation of halogens outside the polar regions may result in depletion of local ozone, along with changes in the chemical budgets of various species in the lower stratosphere (LS). In this paper, both the means and distributions of NO<sub>2</sub> measurements from the Stratospheric Aerosol and Gas Experiment III (SAGE3m) are compared to simulations from a coupled climate-chemistry model, in order to better characterize and quantify subpolar heterogeneous halogen chemistry. Observations of NO<sub>2</sub> from SAGE3m are found to be drawn from the same distribution as the model simulation with heterogeneous chemistry, but from a different distribution than the simulation without heterogeneous chemistry. Results indicate that heterogeneous chemistry plays a significant role in determining the chemical composition of the subpolar LS and show how analysis of distribution functions can provide useful insights to chemical processes.

## Hosted file

zambri\_si.docx available at <https://authorea.com/users/556350/articles/606406-subpolar-activation-of-halogen-heterogeneous-chemistry-in-austral-spring>

1                   **Subpolar activation of halogen heterogeneous chemistry in austral spring**

2                   Brian Zambri<sup>1</sup>, Douglas E. Kinnison<sup>2</sup>, and Susan Solomon<sup>1</sup>

3                   <sup>1</sup>Department of Earth, Atmospheric, and Planetary Sciences, Massachusetts Institute of  
4                   Technology, Cambridge, MA, USA

5                   <sup>2</sup>Atmospheric Chemistry Observations and Modeling Laboratory, National Center for  
6                   Atmospheric Research, Boulder, CO, USA

7                   Submitted to *Geophysical Research Letters*

8                   July 2020

9   **Key points:**

- 10           • NO<sub>2</sub> depletion in observations and model simulations indicate significant heterogeneous  
11           halogen activation in the Southern Hemisphere subpolar lower stratosphere.
- 12           • Novel evidence for chemical processes is revealed using not just means but also  
13           probability distributions in NO<sub>2</sub> data versus simulations.
- 14           • Inclusion of heterogeneous chemical processes is essential for model simulations to  
15           faithfully reproduce the NO<sub>2</sub> distributions observed in this region.

16   *Correspondence to:*

17   Brian Zambri

18   Department of Earth, Atmospheric, and Planetary Sciences

19   Massachusetts Institute of Technology

20   77 Massachusetts Avenue

- 21 Cambridge, MA 02139
- 22 Email: [bzambri@mit.edu](mailto:bzambri@mit.edu)

## ABSTRACT

23  
24 Heterogeneous halogen chemistry plays a dominant role in driving changes in polar chemical  
25 composition and ozone depletion. Activation of halogens outside the polar regions may result in  
26 depletion of local ozone, along with changes in the chemical budgets of various species in the  
27 lower stratosphere (LS). In this paper, both the means and distributions of NO<sub>2</sub> measurements  
28 from the Stratospheric Aerosol and Gas Experiment III (SAGE3m) are compared to simulations  
29 from a coupled climate-chemistry model, in order to better characterize and quantify subpolar  
30 heterogeneous halogen chemistry. Observations of NO<sub>2</sub> from SAGE3m are found to be drawn  
31 from the same distribution as the model simulation with heterogeneous chemistry, but from a  
32 different distribution than the simulation without heterogeneous chemistry. Results indicate that  
33 heterogeneous chemistry plays a significant role in determining the chemical composition of the  
34 subpolar LS and show how analysis of distribution functions can provide useful insights to  
35 chemical processes.

36 **Plain Language Summary.** Much research has been done on the impacts of ozone-depleting  
37 substances on the atmospheres of the polar regions, where their impacts, including the infamous  
38 Antarctic ozone hole, are greatest. However, it is possible for these same chemicals to be active  
39 outside the polar regions, where they can destroy ozone locally as they do near the poles. In this  
40 study, we analyze observations of NO<sub>2</sub> outside the polar region. Because its concentrations are  
41 also impacted by the same chemistry that destroys ozone, NO<sub>2</sub> is a good indicator of where  
42 chemistry involving ozone-depleting substances is occurring. We provide important evidence for  
43 the active presence of ozone-depleting substances outside of the polar regions. In addition, we  
44 use a model to show that the chemistry is essential to explain the observed NO<sub>2</sub> distributions.

45 The results presented here should motivate further research on the impacts of ozone-depleting  
46 substances on ozone abundances throughout the atmosphere.

## 47 1. Introduction

48 It is well known that heterogeneous halogen chemistry in and on polar stratospheric  
49 particles (PSCs) plays a dominant role in driving changes in polar chemical composition (e.g.,  
50 ClO, HCl, ClONO<sub>2</sub>, NO<sub>2</sub>) and ozone depletion. While such processes could also be important  
51 outside the polar regions, their impacts there are smaller and therefore more difficult to identify  
52 (see, e.g., Solomon, 1999, and references therein). Significant activation of inorganic halogens  
53 outside the polar regions may potentially result in the following: (i) depletion of ozone, including  
54 possible chemistry-climate coupling (e.g., Hanson et al., 1994; Anderson et al., 2017), (ii)  
55 changes in the chemical budgets not only of chlorine and bromine species, but also those of  
56 nitrogen compounds in the upper troposphere and lower stratosphere (Adams et al., 2017;  
57 Solomon et al., 2016; Zambri et al., 2019); and (iii) alteration of the local loss rates and lifetimes  
58 of some organic molecules due to enhanced atomic chlorine concentrations, e.g., C<sub>2</sub>H<sub>6</sub> and  
59 methane near the tropopause (Lelieveld et al., 1999). These considerations broaden the scope of  
60 potential impacts associated with the chemistry of the subpolar stratosphere.

61 Anderson et al. (2012, 2017) theorized potential roles of liquid sulfate aerosols for ozone  
62 loss under cold tropopause conditions at mid-latitudes along with changes in water vapor  
63 associated with deep convection. Solomon et al. (2016) used model calculations to argue that  
64 heterogeneous halogen activation may occur near the tropical monsoon regions as well. Near the  
65 mid-latitude tropopause, some modeling studies have suggested that heterogeneous chemistry  
66 might also occur on cirrus cloud particles (e.g., Borrmann et al., 1996; Solomon et al., 1997). A  
67 number of observational studies have made use of volcanic perturbations to provide airborne  
68 and/or satellite evidence for reductions in NO<sub>x</sub> associated with liquid sulfate aerosol chemistry

69 (e.g., Fahey et al., 1993; Adams et al., 2017; Zambri et al., 2019) but the specific reactions  
70 involved and their chemical impacts are not fully established. Important evidence has been  
71 presented for heterogeneous halogen chemistry in the tropopause region outside the polar  
72 vortices, but its scope and impacts remain uncertain (e.g., Thornton et al., 2003; Santee et al.,  
73 2011; Barrera et al., 2020) and additional study, especially with satellite methods that can  
74 provide extensive temporal and latitudinal coverage, is useful.

75 In this study, we analyze the chemistry of the Southern Hemisphere (SH) subpolar lower  
76 stratosphere using satellite observations from the Stratospheric Aerosol and Gas Experiment III  
77 on the Meteor-3M satellite (SAGE3m) in conjunction with the National Center for Atmospheric  
78 Research (NCAR) Community Earth System Model, version 2 (CESM2) Whole Atmosphere  
79 Community Climate Model (WACCM6; Danabasoglu et al., 2020; Gettelman et al., 2019). The  
80 model is run in specified dynamics (SD) mode wherein an observations-based reanalysis  
81 provides the temperatures and winds that are important for the chemistry.  $\text{NO}_2$  is a useful  
82 indicator of heterogeneous processes. Reactions on surfaces (Solomon et al., 2015) convert  $\text{NO}_2$   
83 from short-lived  $\text{NO}_x$  reservoir species to longer-lived reservoir species, thereby locally  
84 depleting  $\text{NO}_2$  and “denoxifying” the atmosphere. Some heterogeneous processes result only in  
85 denoxification (e.g.,  $\text{N}_2\text{O}_5 + \text{H}_2\text{O} \rightarrow 2\text{HNO}_3$ ) and indirectly affect halogens, while others not only  
86 denoxify but also directly activate halogens from longer-lived species to more reactive forms  
87 (e.g.,  $\text{HCl} + \text{ClONO}_2 \rightarrow \text{HNO}_3 + \text{Cl}_2$ ). Therefore,  $\text{NO}_2$  abundances are a key tool for analysis of  
88 heterogeneous processing and evaluation of chemical understanding. We show how comparisons  
89 of not just means but more importantly the modeled and observed  $\text{NO}_2$  distributions, defined by  
90 their discrete probability density functions (PDF) can be expected to demonstrate *where, when,*  
91 *and by how much heterogeneous halogen chemistry can perturb chemical composition outside*

92 *the polar vortex*. The analysis of probability distributions is shown to be a useful tool, and can  
93 also be expected to improve understanding of the measurement capabilities (including sensitivity  
94 and precision).

## 95 **2. Materials and Methods**

### 96 **2.1 SAGE3m**

97 The SAGE III was launched aboard the Russian Aviation and Space Agency's Meteor-  
98 3M satellite (Mauldin et al., 1998). The satellite was launched on December 10, 2001 into a Sun-  
99 synchronous orbit at an altitude of 1020 km and with an approximate 9:00 a.m. equatorial  
100 crossing time on the ascending node. The occultation instrument provided NO<sub>2</sub> measurements at  
101 0.5-km vertical resolution from the tropopause to 45 km from 2002 to 2005, mostly at high  
102 latitudes in the Northern Hemisphere (between 50° and 80°N) and midlatitudes in the Southern  
103 Hemisphere (between 30° and 50°S). SAGE3m NO<sub>2</sub> observations are interpolated vertically to  
104 the CESM2(WACCM) grid.

### 105 **2.2 CESM2(WACCM)**

106 The CESM2(WACCM6) is the latest version of the CESM (Danabasoglu et al., 2020;  
107 Gettelman et al., 2019). The configuration of CESM2(WACCM) used here features ~2° (1.9°  
108 latitude × 2.5° longitude) horizontal resolution and a finite volume dynamical core (Lin & Rood,  
109 1997). The model was run in specified dynamics mode (WACCM-SD) using the National  
110 Aeronautics and Space Administration Global Modeling and Assimilation Office Modern-Era  
111 Retrospective analysis for Research and Applications, Version 2 (MERRA2) meteorological  
112 fields (Gelaro et al., 2017). WACCM-SD allows for the synoptic comparison of model and

113 observations; in particular, WACCM has a purpose-built capability to output chemical  
114 constituent and other information at the specific longitude, latitude, and local time of a given  
115 satellite instrument. This tool has been employed in previous studies, for example, to examine  
116 sunrise and sunset data for ClONO<sub>2</sub> and O<sub>3</sub> (Sakazaki et al., 2015; Solomon et al., 2015). We  
117 have leveraged this capability to extract the model output at the same times and locations as the  
118 SAGE3m observations, which allows for a like-like comparison of model and observations.

### 119 **2.3 Defining the subpolar region**

120         The stratospheric polar vortex is a large-scale region of air that is contained by strong  
121 westerly winds that circle the polar region. This westerly jet stream is usually referred to as the  
122 polar night jet. The polar vortex extends from the tropopause through the stratosphere and into  
123 the mesosphere (above 50 km; Waugh, Sobel & Polvani, 2017). Cold temperatures and low  
124 ozone abundances, relative to midlatitudes, are associated with the air inside the vortex, because  
125 the polar vortex inhibits the exchange of polar and midlatitude air (Fig. 1). The potential vorticity  
126 (PV) is a conserved quantity that acts as a tracer for motion on an isentropic surface and is  
127 frequently used to distinguish polar versus midlatitude airmasses, although the vortex is not  
128 completely impermeable. In the winter, the magnitude of the PV is larger at the pole than at  
129 midlatitudes. The spacing of PV contours is tightest at the polar vortex edge, and widens inside  
130 the vortex and at latitudes equatorward of the vortex edge. The edge of the vortex is therefore  
131 defined to be where the contours of PV are closest together, quantified as the location of the  
132 maximum PV gradient with respect to equivalent latitude (Nash et al., 1996). In order to identify  
133 activation of inorganic halogens and heterogeneous chemistry, we consider only profiles that are

134 outside the vortex and within  $8^\circ$  of the polar vortex edge for a given day. Fig. 1 illustrates the  
135 selection of “subpolar” SAGE3m retrievals for October 29, 2014.

## 136 **2.4 Comparison of observed and modelled NO<sub>2</sub> distributions**

137 In order to compare the NO<sub>2</sub> distributions based on SAGE3m observations and the  
138 CESM2(WACCM) simulations with (WACCMhet) and without (WACCMnohet) heterogeneous  
139 chemistry, we use the two-sample Kolmogorov–Smirnov test (K–S test; Smirnov, 1948). The  
140 two-sample K–S statistic is given by

$$141 \quad D = \max_x |F_1(x) - F_2(x)|, \#(1)$$

142 where  $F_1$  and  $F_2$  are the empirical distribution functions (ECDF) of the respective samples. The  
143 K–S test measures the maximum distance between the empirical distributions; the two data  
144 samples are deemed to be drawn from different distributions (i.e., the null hypothesis rejected) at  
145 level  $\alpha$  if the distance,  $D$ , is smaller than some critical value,  $c(\alpha, n_1, n_2)$ , where  $n_1$  and  $n_2$  are  
146 the sample sizes. The K–S test statistic is illustrated in Fig. 2, which shows an example of  
147 distributions of NO<sub>2</sub> for SAGE3m (black), WACCMhet (blue), and WACCMnoHet (red), where  
148 vertical dashed lines indicate the different values of  $D$ . As discussed further below, in the UTLS  
149 region the polar vortex is not as strong a barrier between polar and subpolar air, and so we also  
150 include the results of a simulation in which the heterogeneous chemical reactions were turned off  
151 only poleward of  $60^\circ\text{N/S}$  (WACCMnoHet60NS; green line in Figs. 2–3) to identify the extent to  
152 which mixing may impact the observed and modelled NO<sub>2</sub> distributions.

## 153 **3. Results**

154 Fig. 3 shows ~1000 subpolar NO<sub>2</sub> profiles for September and October for the SAGE3m  
155 observations and WACCM model simulations, as well as their relative frequencies of NO<sub>2</sub>  
156 concentrations in the UTLS (164–72 hPa). It is evident that SAGE3m and WACCMhet NO<sub>2</sub>  
157 abundances are broadly consistent. Note the occurrence of a substantial number of low values of  
158 NO<sub>2</sub> from ~50 hPa down to near the tropopause in both observations and model results, although  
159 it is more apparent in the model where values can be lower than 10 pptv (likely below the  
160 detection limit of the SAGE3m instrument). For this reason, we are less interested in the extreme  
161 low values of NO<sub>2</sub> and more interested in the values near 50–100 pptv, which are within the  
162 measurement range of good estimated accuracy of the observations. Comparison of Fig. 3b  
163 (WACCMhet) and Fig. 3c (WACCMnoHet) shows a stark change in NO<sub>2</sub> abundances based on  
164 the inclusion of heterogeneous chemical processes. The absence of low NO<sub>2</sub> abundances in  
165 WACCMnoHet (Fig. 3d) relative to observations (Fig. 3a) and WACCMhet (Fig. 3b) is a direct  
166 indication of heterogeneous halogen activation in this region. As more NO<sub>2</sub> in halogen nitrates is  
167 converted to HNO<sub>3</sub>, this not only depletes NO<sub>2</sub>, but it also increases the availability of ClO there  
168 and can deplete ozone, making such observations of NO<sub>2</sub> an important indicator for chemistry  
169 related to ozone depletion.

170 Fig. 3e shows the PDF approach: we first collect all the data points for sampled profile  
171 observations and model simulations between 164 hPa and 72 hPa, as in the region denoted in  
172 Figs. 3a–d in the heart of the heterogeneous activation. The relative frequencies are constructed  
173 in 25 pptv bins. The observations (black) and model results with heterogeneous chemistry (blue)  
174 are overall in very good agreement. For 25–100 pptv, the normalized frequencies are higher in  
175 the observations relative to the model. On the other hand, the model suggests a higher frequency

176 of occurrence of values below 25 pptv than the data. Again, instrument sensitivity may be an  
177 issue in terms of observation of these very low NO<sub>2</sub> concentrations.

178         Similar to Figs. 3a–d, the WACCMnoHet simulation PDF exhibits a large decrease in the  
179 probability of NO<sub>2</sub> values less than 125 pptv, compared to both the observed and WACCMhet  
180 PDFs (Fig. 3e). This is a qualitative but clear indication that heterogeneous activation is indeed  
181 occurring. Furthermore, the observations and WACCMhet are in broad agreement. It is also  
182 important to note that there is a higher probability of NO<sub>2</sub> in the WACCMnoHet simulation in  
183 the higher magnitude NO<sub>2</sub> bins (relative to the WACCMhet simulation and observations). This is  
184 consistent with more available NO<sub>2</sub> shifting the distribution towards 200 pptv and higher. These  
185 results are not sensitive to the model horizontal resolution, as WACCMhet simulations at 1° yield  
186 almost identical distributions (Fig. S1).

187         Though we have excluded retrievals inside the polar vortex, the vortex edge at these  
188 altitudes is not as efficient a barrier to transport and mixing of polar and subpolar air as at higher  
189 altitudes (McIntyre, 1995), and so the chemical composition of subpolar air at these latitudes is  
190 subject to greater exchange between polar and midlatitude air (Tuck, 1989). Therefore, the  
191 denoxification in the LS in Figure 3 is due to a combination of heterogeneous activation outside  
192 the polar vortex and chemical processing inside and subsequent transport outside of the polar  
193 vortex. This is illustrated in Figs. 3c, e: WACCMnoHet60NS shows lower frequencies of NO<sub>2</sub>  
194 concentrations below 100 pptv and higher frequencies of concentrations in the 100–200 pptv  
195 concentration, relative to WACCMHet.

196         For a more quantitative comparison of the NO<sub>2</sub> distributions, Fig. 2 shows the ECDFs for  
197 the observations and three model simulations. The vertical lines indicate the maximum distances

198 between each of the distributions, which is equivalent to the K–S test statistic. It is clear that the  
199 WACCMnoHet distribution (red) is different from the others, with the null hypothesis of the K–  
200 S test being rejected at the  $\alpha = 0.00001$  level in all three cases (that is, the probability of  
201 WACCMnoHet NO<sub>2</sub> being drawn from the same distribution as SAGE3m (black), WACCMhet  
202 (blue), or WACCMnoHet60NS (green) is  $p < 0.00001$ ). On the other hand, SAGE3m and  
203 WACCMhet NO<sub>2</sub> are drawn from the same distribution, with the K–S test failing to reject the  
204 null hypothesis at the  $\alpha = 0.05$  level. WACCMnoHet60NS is drawn from the same distribution  
205 as WACCMhet at the  $\alpha = 0.1$  level, indicating that much of the heterogeneous activation  
206 evidenced by low NO<sub>2</sub> concentrations in WACCMhet is occurring at subpolar latitudes.  
207 However, WACCMnoHet60NS is drawn from a different distribution than SAGE3m: the null  
208 hypothesis is rejected with  $p < 0.00001$ ; this further indicates that the exchange of polar-  
209 processed air with midlatitude air also contributes to the SAGE3m observed and WACCMhet  
210 NO<sub>2</sub> distributions.

211 In contrast to the clear heterogeneous halogen activation illustrated by the NO<sub>2</sub>  
212 distributions in the lower stratosphere, Fig. 4 shows the PDFs for the middle stratosphere (11–5  
213 hPa), where heterogeneous chemistry is not expected to impact NO<sub>2</sub> concentrations. In this case,  
214 the WACCMhet and WACCMnoHet distributions are nearly identical (Fig. 4a–b), with the K–S  
215 test failing to reject the null hypothesis at the  $\alpha = 0.5$  level. On the other hand, the SAGE3m  
216 NO<sub>2</sub> concentrations are clearly drawn from a different distribution than the model NO<sub>2</sub>  
217 concentrations, given the discrepancies in Figs. 4a–b. However, visual inspection reveals that the  
218 shapes of the distributions are very similar, and the differences reflect an offset. This stands in  
219 contrast to the differences in shape of the distributions found at lower altitudes between the  
220 observations and the WACCMnoHet case. Thus, we suggest that it is most likely that a model–

221 observation bias of  $\sim 570$  pptv (or  $\sim 9\%$ ) is responsible for these apparently “different”  
222 distributions. To demonstrate this, Figs. 4c–d show the same distributions with the WACCM  
223  $\text{NO}_2$  adjusted to have the same mean values as the SAGE3m observations by adding the mean  
224 difference to each WACCM profile. In this case, the three distributions are equal, with the K–S  
225 test failing to reject the null hypothesis at the  $\alpha = 0.25$  level for WACCMhet–SAGE3m, and at  
226 the  $\alpha = 0.5$  level for WACCMnoHet–SAGE3m. This is an important consideration, since it  
227 shows that the scales (i.e., the spreads of the distributions) are alike, and it is the locations (i.e.,  
228 the means) that cause the  $\text{NO}_2$  distributions to be considered different at these levels. This is in  
229 contrast to the UTLS region (Figs. 2–3), for which the SAGE3m observations and  
230 WACCMnoHet simulation are deemed to be drawn from different distributions ( $p < 0.00001$ ),  
231 even after adjusting the means as above (not shown).

#### 232 **4. Summary and Conclusions**

233 Much deserved attention has been given to understanding the role of PSC heterogeneous  
234 halogen chemistry in driving changes in polar atmospheric composition and ozone depletion. In  
235 addition, important evidence has been presented for heterogeneous halogen chemistry outside the  
236 polar vortices (Thornton et al., 2003; Santee et al., 2011), but its scope and impacts have not  
237 been probed. In this study, we have identified substantial and consistent occurrence of such  
238 chemistry outside the polar regions, which broadens the scope of potential impacts associated  
239 with the chemistry of the subpolar stratosphere. While quantitative uncertainties remain (such  
240 as incomplete knowledge of thermal fluctuations potentially associated with sub-grid scale  
241 gravity waves, and of the rates of heterogeneous kinetic processes measured in the laboratory,

242 etc.), the approach of analyzing probability distribution functions from models and satellite  
243 observations has been shown to provide an improved picture of key aspects of this chemistry.

244 In particular, we have shown that: (1) there is strong evidence for considerable  
245 heterogeneous halogen activation occurring locally in the subpolar lower stratosphere in  
246 September–October, as illustrated by the occurrence of extremely low NO<sub>2</sub> concentrations; (2)  
247 concentrations of NO<sub>2</sub> from observations and model simulations with heterogeneous chemistry  
248 turned on are drawn from the same distribution, and the inclusion of heterogeneous chemistry at  
249 both subpolar and polar latitudes appears to be *essential* for model–observation agreement; (3) at  
250 higher altitudes, where there is no heterogeneous activation, the model simulations with and  
251 without heterogeneous chemistry are nearly identical, and show the same scale (spread) as the  
252 observations, though the mean of the observations is about 9% higher than the model.

253 These results indicate that heterogeneous activation of halogens could play a role in  
254 ozone variability and trends in the subpolar lower stratosphere that is thus-far unaccounted for. It  
255 also highlights the importance of examining not only the mean state of atmospheric composition,  
256 but also its distribution. Overall, these results act to enhance understanding of heterogeneous  
257 chemical processes and their impacts in the stratosphere.

258 **Acknowledgments.** BZ and DK were funded in part by NASA grant (80NSSC19K0952). BZ and  
259 SS were funded in part by NSF 1906719. This research was enabled by the computational and  
260 storage resources of NCAR's Computational and Information Systems Laboratory (CISL),  
261 sponsored by the NSF. Cheyenne: HPE/SGI ICE XA System (NCAR Community Computing).  
262 Boulder, CO: National Center for Atmospheric Research. <https://doi.org/10.5065/D6RX99HX>

263  
264 **Data Availability.** Model output used is available at <https://doi.org/10.7910/DVN/PIYPBB>.  
265 MERRA2 reanalysis data are available at  
266 [https://disc.gsfc.nasa.gov/datasets?keywords=%22MERRA-](https://disc.gsfc.nasa.gov/datasets?keywords=%22MERRA-2%22&page=1&source=Models%2FAnalyses%20MERRA-2)  
267 [2%22&page=1&source=Models%2FAnalyses%20MERRA-2](https://disc.gsfc.nasa.gov/datasets?keywords=%22MERRA-2%22&page=1&source=Models%2FAnalyses%20MERRA-2). SAGE satellite data is available at  
268 [https://eosweb.larc.nasa.gov/project/sage3/sage3\\_table](https://eosweb.larc.nasa.gov/project/sage3/sage3_table).

## References

- 269  
270 Adams, C., Bourassa, A. E., McLinden, C. A., Sioris, C. E., Clarmann, T. V., Funke, B., Rieger,  
271 L. A., & Degenstein, D. A. (2017). Effect of volcanic aerosol on stratospheric NO<sub>2</sub> and  
272 N<sub>2</sub>O<sub>5</sub> from 2002–2014 as measured by Odin-OSIRIS and Envisat-MIPAS. *Atmos. Chem.*  
273 *Phys.*, 17(13), 8063–8080. <https://doi.org/10.5194/acp-17-8063-2017>
- 274 Anderson, J. G., Wilmouth, D. M., Smith, J. B., & Sayres, D. S. (2012). UV dosage levels in  
275 summer: Increased risk of ozone loss from convectively injected water vapor. *Science*,  
276 337, 835–839. <https://doi.org/10.1126/science.1222978>
- 277 Anderson, J. G., Weisenstein, D. K., Bowman, K. P., Homeyer, C. R., Smith, J. B., Wilmouth, D.  
278 M., Sayres, D. S., et al. (2017). Stratospheric ozone over the United States in summer  
279 linked to observations of convection and temperature via chlorine and bromine catalysis.  
280 *Proc. Nat. Acad. Sci.*, 114, E4905–E4913. <https://doi.org/10.1073/pnas.1619318114>
- 281 Barrera, J. A., Fernandez, R. P., Iglesias-Suarez, F., Cuevas, C. A., Lamarque, J. –F., & Saiz-  
282 Lopez, A (2020). Seasonal impact of biogenic very short-lived bromocarbons on  
283 lowermost stratospheric ozone between 60°N and 60°S during the 21<sup>st</sup> century. *Atmos.*  
284 *Chem. Phys.*, 20, 8083–8102. <https://doi.org/10.5194/acp-20-8083-2020>
- 285 Borrmann, S., Solomon, S., Dye, J. E., & Luo, B. (1996). The potential of cirrus clouds for  
286 heterogeneous chlorine activation. *Geophys. Res., Lett.*, 23(16), 2133–2136.
- 287 Chu, W. P., Trepte, C. R., Veiga, R. E., Cisewski, M. S., & Taha, G. (2002). SAGE III  
288 measurements, *Proc. SPIE*, 4814. <https://doi.org/10.1117/12.451515>
- 289 Danabasoglu, G., Lamarque, J.-F., Bacmeister, J., Bailey, D. A., DuVivier, A. K., Edwards, J., et  
290 al. (2020). The Community Earth System Model Version 2 (CESM2). *Journal of*  
291 *Advances in Modeling Earth Systems*, 12, e2019MS001916.  
292 <https://doi.org/10.1029/2019MS001916>
- 293 Fahey, D. W., Kawa, S. R., Woodbridge, E. L., Tin, P., Wilson, J. C., Jonsson, H. H., Dye, J. E.,  
294 et al. (1993). Heterogeneous chemistry in the mid-latitude lower stratosphere: The role of  
295 reactive nitrogen and the impact of volcanic aerosol in ozone photochemistry. *Nature*,  
296 363, 509–514.
- 297 Gelaro, R., McCarty, W., Suárez, M. J., Todling, R., Molod, A., Takacs, L., et al. (2017). The  
298 Modern-Era Retrospective Analysis for Research and Applications, Version 2 (MERRA-  
299 2). *Journal of Climate*, 30(14), 5419–5454. <https://doi.org/10.1175/JCLI-D-16-0758.1>
- 300 Gettelman, A., Mills, M. J., Kinnison, D. E., Garcia, R. R., Smith, A. K., Marsh, D. R., et al.  
301 (2019). The whole atmosphere community climate model version 6 (WACCM6). *Journal*  
302 *of Geophysical Research: Atmospheres*, 124, 12,380–12,403.  
303 <https://doi.org/10.1029/2019JD030943>.
- 304 Hanson, D. R., Ravishankara, A. R., & Solomon, S. (1994). Heterogeneous reactions in sulfuric  
305 acid aerosols: A framework for model calculations. *J. Geophys. Res.*, 99(D2), 3615–3629.
- 306 Lelieveld, J., Bregman, A., Scheeren, H. A., Strom, J., Carslaw, K. S., Fischer, H., Siegmund, P.  
307 C., & Arnold, F. (1999). Chlorine activation and ozone destruction in the northern  
308 lowermost stratosphere. *J. Geophys. Res.*, 104(D7), 8201–8213.
- 309 Lin, S. J., & Rood, R. B. (1997). An explicit Flux-Form Semi-Lagrangian shallow water model  
310 on the sphere. *Quarterly Journal of the Royal Meteorological Society*, 123, 2477–2498.
- 311 Mauldin, L., Salikhov, R., Habib, S., Vladimirov, A., Carraway, D., Petrenko, G., & Comella, J.  
312 (1998). Meteor-3M(1)/Stratospheric Aerosol and Gas Experiment III (SAGE III): Jointly  
313 Sponsored by the National Aeronautics and Space Administration and the Russian Space  
314 Agency. *Proc. SPIE*, 3501, 355–365.

315 Nash, E. R., Newman, P. A., Rosenfield, J. E., & Schoeberl, M. R. (1996). An objective  
316 determination of the polar vortex using Ertel's potential vorticity. *J. Geophys. Res.*,  
317 *101*(D5), 9471–9478. <https://doi.org/10.1029/96JD00066>

318 Sakazaki, T., Shiotani, M., Suzuki, M., Kinnison, D. E., Zawodny, J. M., McHugh, M., &  
319 Walker, K. A. (2015). Sunset–sunrise difference in solar occultation ozone measurements  
320 (SAGE II, HALOE, and ACE–FTS) and its relationship to tidal vertical winds. *Atmos.*  
321 *Chem. Phys.*, *15*, 829–843. <https://doi.org/10.5194/acp-15-829-2015>

322 Santee, M. L., Manney, G. L., Livesey, N. J., Froidevaux, L., Schwartz, M. J., & Read, W. G.  
323 (2011). Trace gas evolution in the lower stratosphere from Aura Microwave Limb  
324 Sounder measurements. *J. Geophys. Res.*, *116*, D18306,  
325 <https://doi.org/10.1029/2011JD015590>

326 Solomon, S., Borrmann, S., Garcia, R. R., Portmann, R., Thomason, L., Poole, L. R. Winker, D.,  
327 & McCormick, M. P. (1997). Heterogeneous chlorine chemistry in the tropopause region.  
328 *J. Geophys. Res.*, *102*, 21411–21429.

329 Solomon, S. (1999). Stratospheric ozone depletion: A review of concepts and history. *Rev.*  
330 *Geophys.*, *37*, 275–316. <https://doi.org/10.1029/1999RG900008>

331 Solomon, S., Kinnison, D., Bandoro, J., & Garcia, R. R. (2015). Polar ozone depletion: An  
332 update. *J. Geophys. Res. Atmos.*, *120*, 7958–7974. <https://doi.org/10.1002/2015JD023365>

333 Solomon, S., Kinnison, D. E., Garcia, R. R., Bandoro, J., Mills, M., Wilka, C., Neely III, R. R.,  
334 et al. (2016). Monsoon circulations and tropical heterogeneous chlorine chemistry in the  
335 stratosphere. *Geophys. Res. Lett.*, *43*(24), 12,624–12,633.  
336 <https://doi.org/10.1002/2016GL071778>

337 Solomon, S., Ivy, D., Gupta, M., Bandoro, J., Santer, B., Fu, Q., Garcia, R. R., et al. (2017).  
338 Mirrored changes in Antarctic ozone and stratospheric temperature in the late 20th versus  
339 early 21st centuries. *J. Geophys. Res.* <https://doi.org/10.1002/2017JD026719>

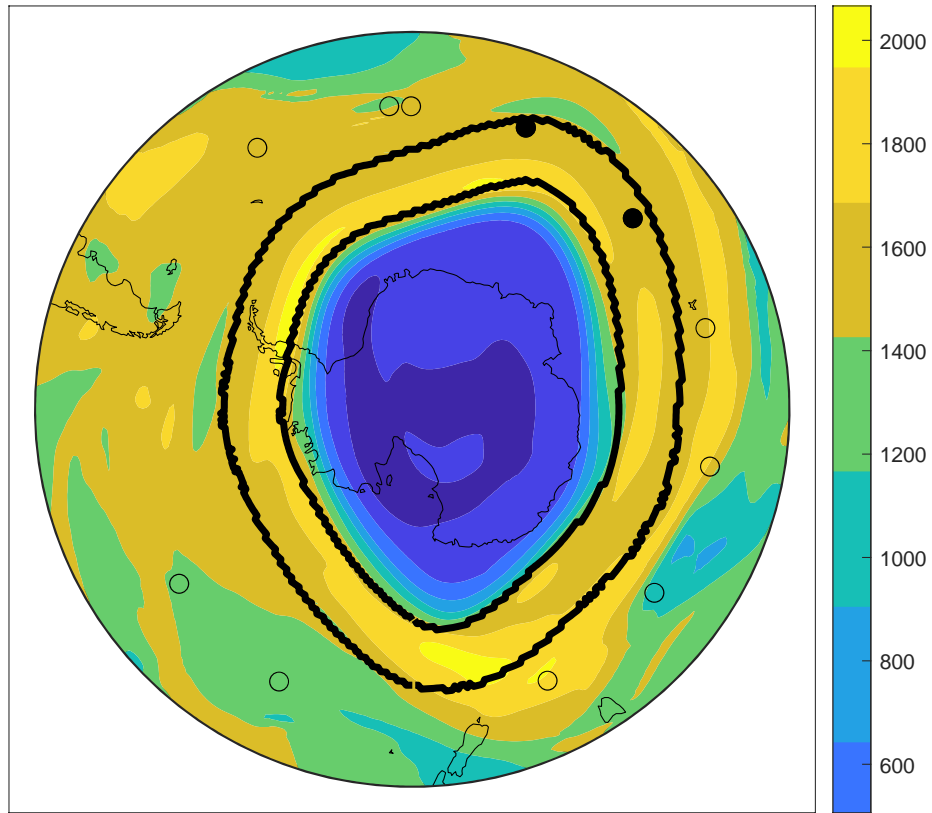
340 Smirnov, N. (1948). Table for estimating the goodness of fit of empirical distributions. *Annals of*  
341 *Mathematical Statistics*, *19*(2), 279–281. <https://doi.org/10.1214/aoms/1177730256>

342 Thornton, B. F., Toohey, D. W., Avallone, L. M., Harder, H., Martinez, M., Simpas, J. B.,  
343 Brune, W. H., & Avery, A. M. (2003). In situ observations of ClO near the winter polar  
344 tropopause. *J. Geophys. Res.*, *108*(D8), 8333. <https://doi.org/10.1029/2002JD002839>

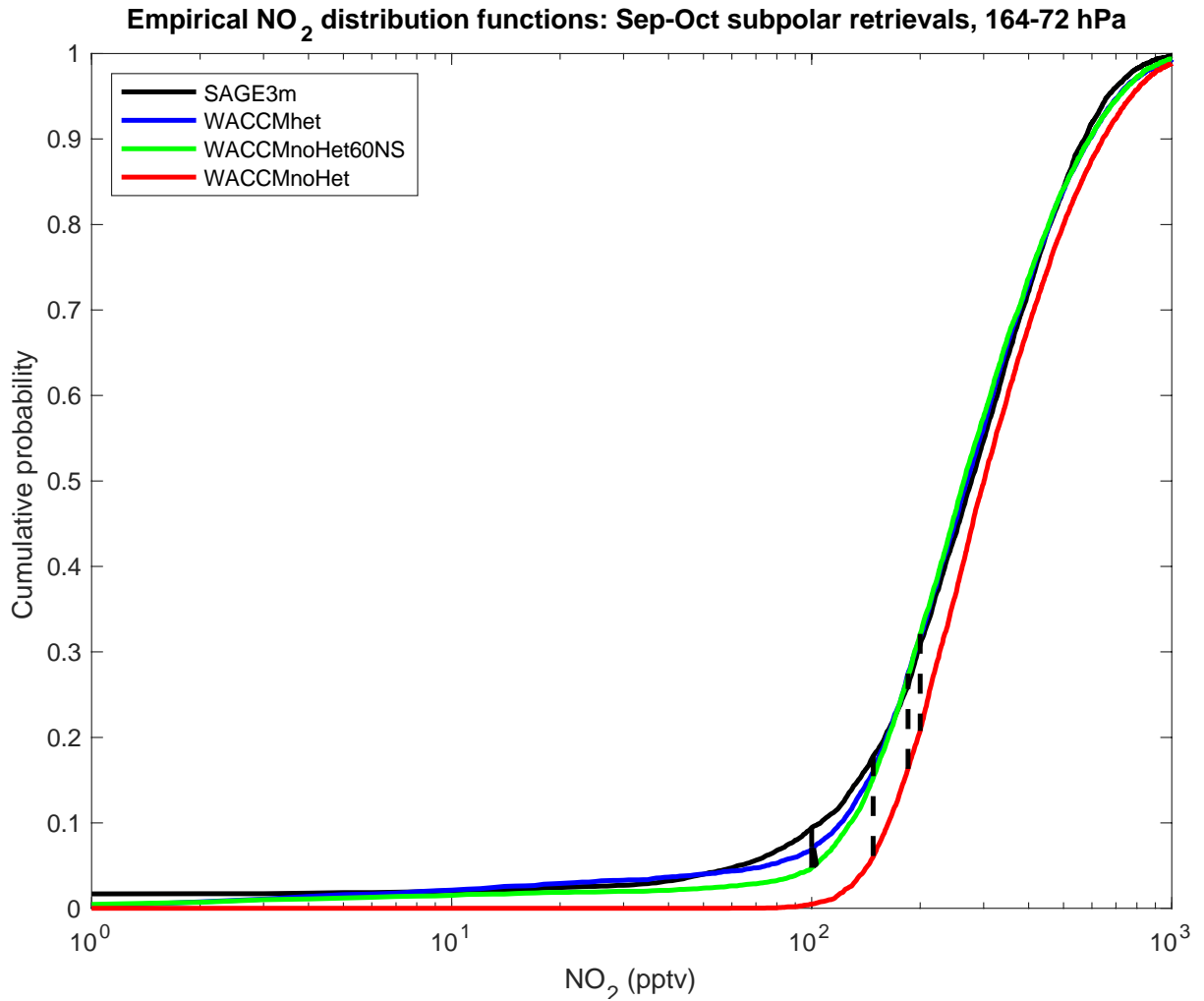
345 Waugh, D. W., Sobel, A. H., & Polvani, L. M. (2017). What is the polar vortex and how does it  
346 influence weather? *Bull. Amer. Met. Soc.*, *98*(1), 37–44. [https://doi.org/10.1175/BAMS-](https://doi.org/10.1175/BAMS-D-15-00212.1)  
347 [D-15-00212.1](https://doi.org/10.1175/BAMS-D-15-00212.1)

348 Zambri, B., Solomon, S., Kinnison, D. E., Mills, M. J., Schmidt, A., Neely, R. R., III, et al.  
349 (2019). Modeled and observed volcanic aerosol control on stratospheric NO<sub>y</sub> and Cl<sub>y</sub>.  
350 *Journal of Geophysical Research: Atmospheres*, *124*.  
351 <https://doi.org/10.1029/2019JD031111>  
352

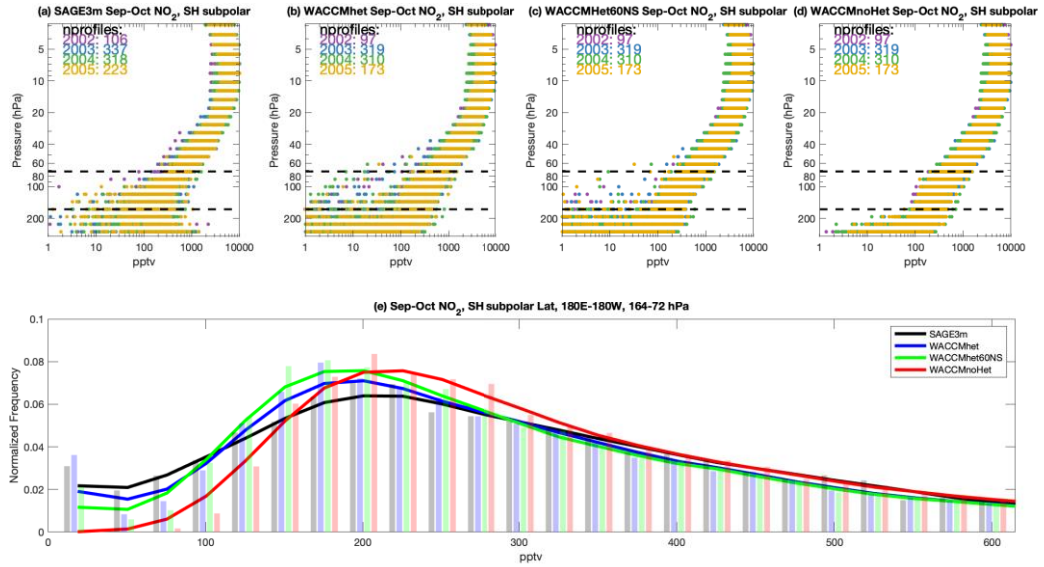
SAGE3m retrievals and MERRA2 O<sub>3</sub> (ppbv) for 20041029



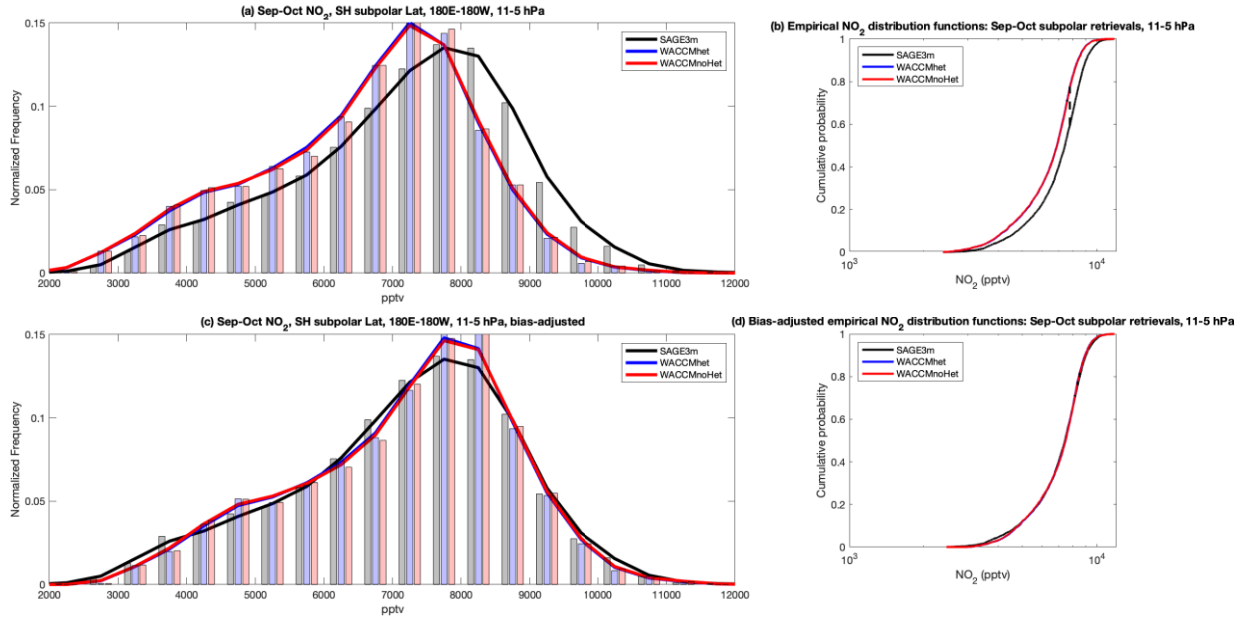
353 **Figure 1.** Locations of SAGE3m retrievals in the Southern Hemisphere for October 29, 2004 as  
354 an example. Black contours indicate the subpolar region as determined by the maximum PV  
355 gradient on the 460 K isentropes on that day. Open and filled circles represent SAGE3m retrievals  
356 that were excluded from and included in the analysis, respectively, based on proximity to the  
357 vortex edge. Also shown are the MERRA2 O<sub>3</sub> concentrations at 460 K, to highlight the changes  
358 in atmospheric composition inside and outside the polar vortex.



359 **Figure 2.** ECDFs for (black) SAGE3m, (blue) WACCMhet, (green) WACCMnoHet60NS, and  
 360 (red) WACCMnoHet. Vertical dashed lines indicate the two-sample K–S test statistics, which are  
 361 the maximum distances between two samples. Distribution functions shown are for September–  
 362 October and 164–72 hPa.



363 **Figure 3.** (a)–(d): September–October NO<sub>2</sub> concentrations for subpolar retrievals for (a)  
 364 SAGE3m, (b) WACCMhet, (c) WACCMhet60NS, and (d) WACCMnoHet. (e) PDFs for 164–72  
 365 hPa for (black) SAGE3m, (blue) WACCMhet, (green) WACCMhet60NS, and (red)  
 366 WACCMnoHet. Horizontal dashed lines in (a)–(d) indicate the vertical range for the  
 367 distributions in (e). Solid lines in (e) are the Epanechnikov kernel density estimates.



368 **Figure 4.** (a) PDFs and (b) ECDFs of September–October NO<sub>2</sub> concentrations for subpolar  
 369 retrievals for 11–5 hPa for (black) SAGE3m, (blue) WACCMhet, and (red) WACCMnoHet. (c)–  
 370 (d): as (a)–(b), but with WACCM means adjusted to match the SAGE3m mean.

Figure 1.

SAGE3m retrievals and MERRA2 O<sub>3</sub> (ppbv) for 20041029

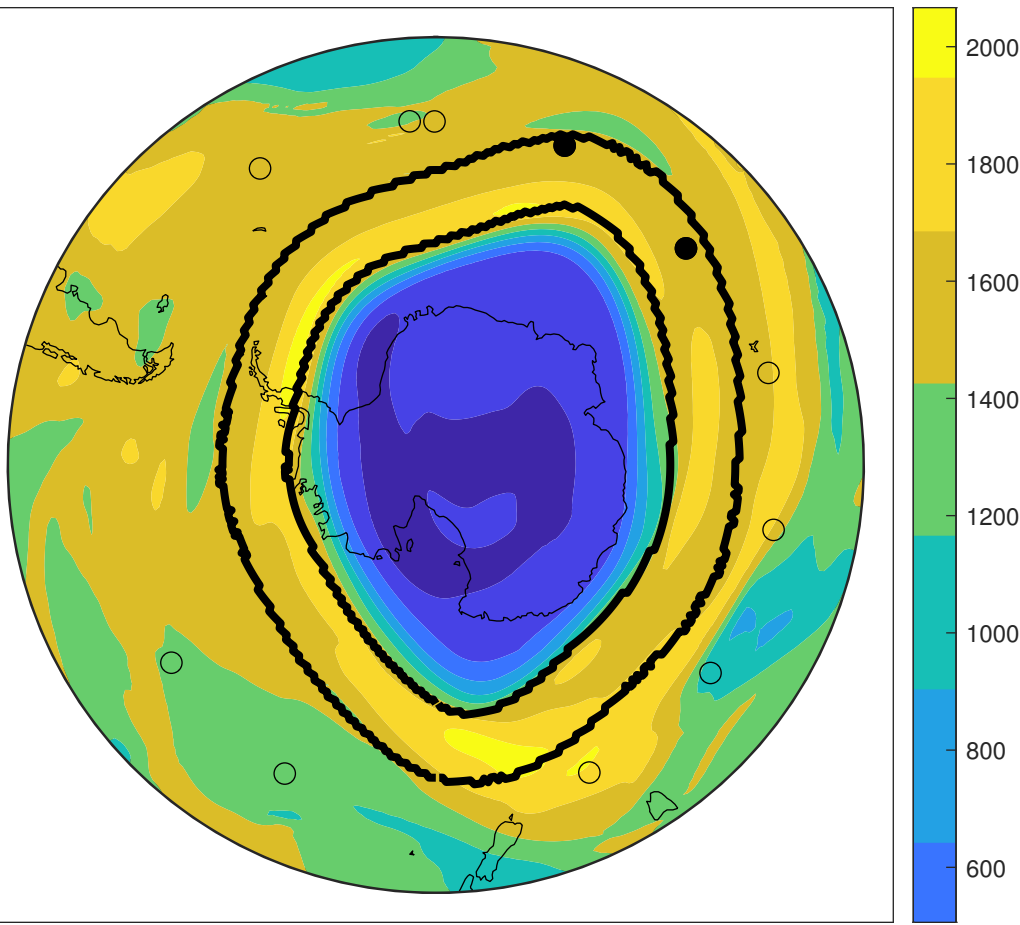


Figure 2.

Empirical  $\text{NO}_2$  distribution functions: Sep-Oct subpolar retrievals, 164-72 hPa

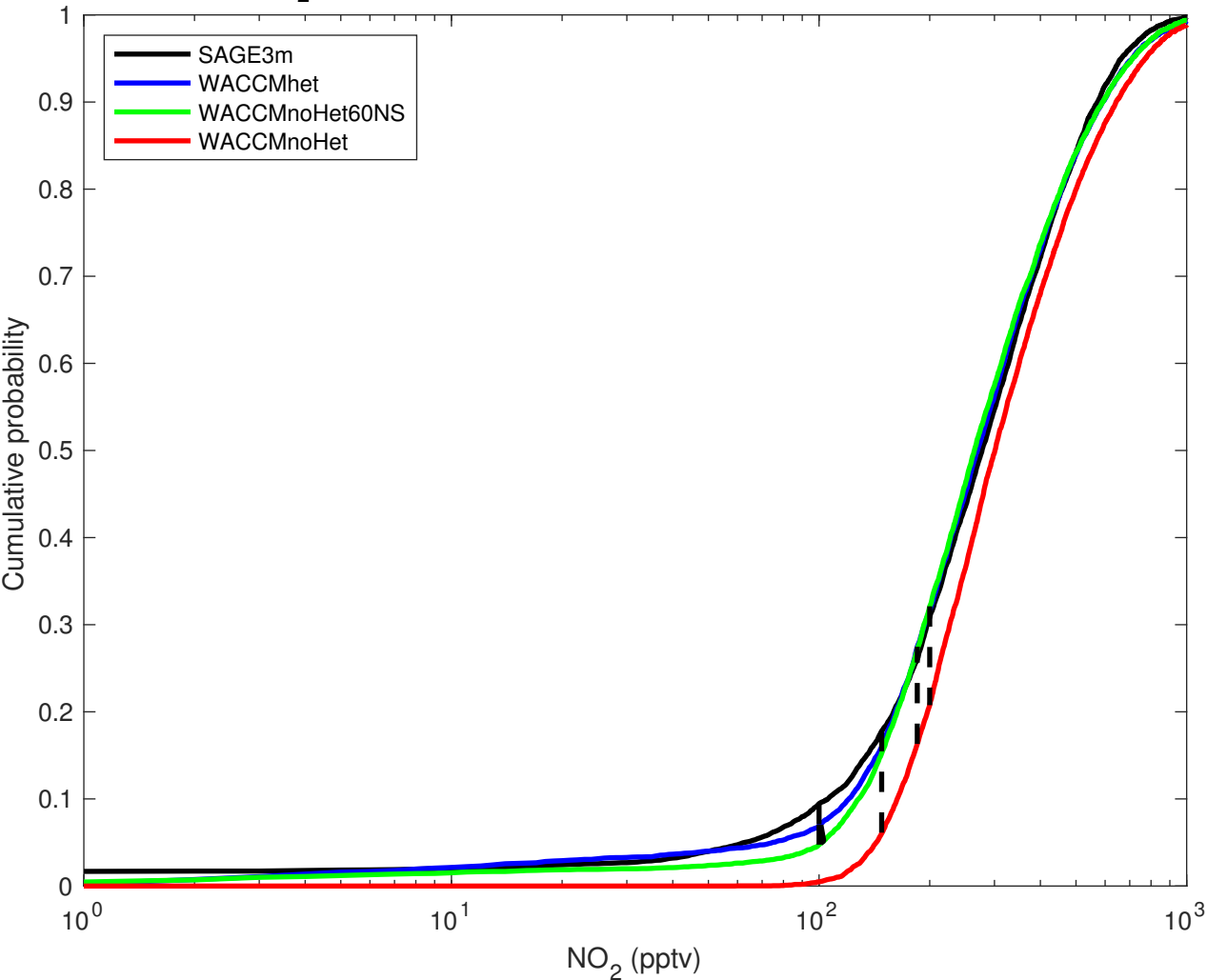
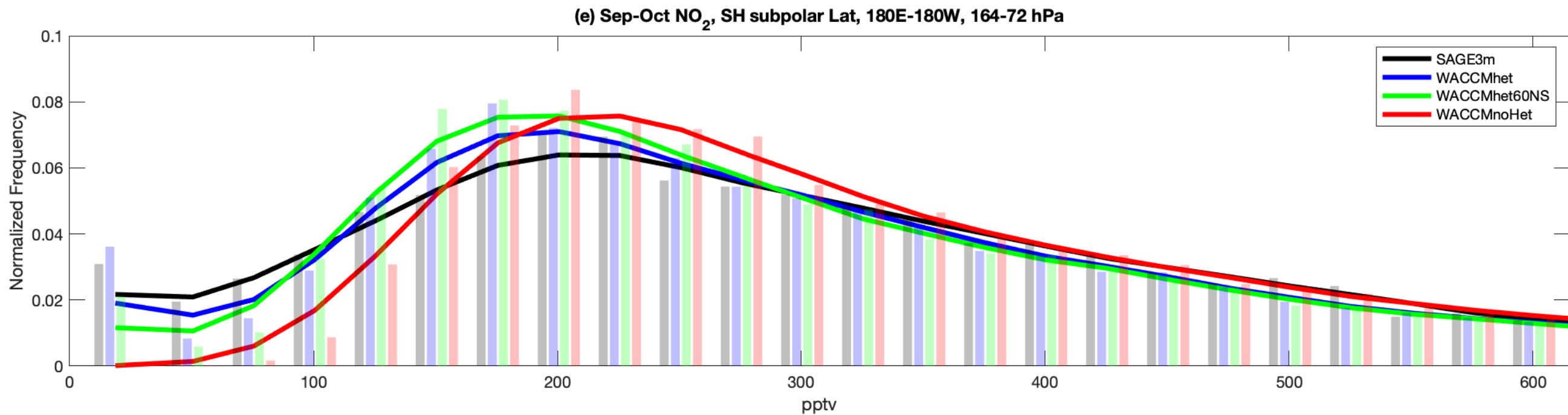
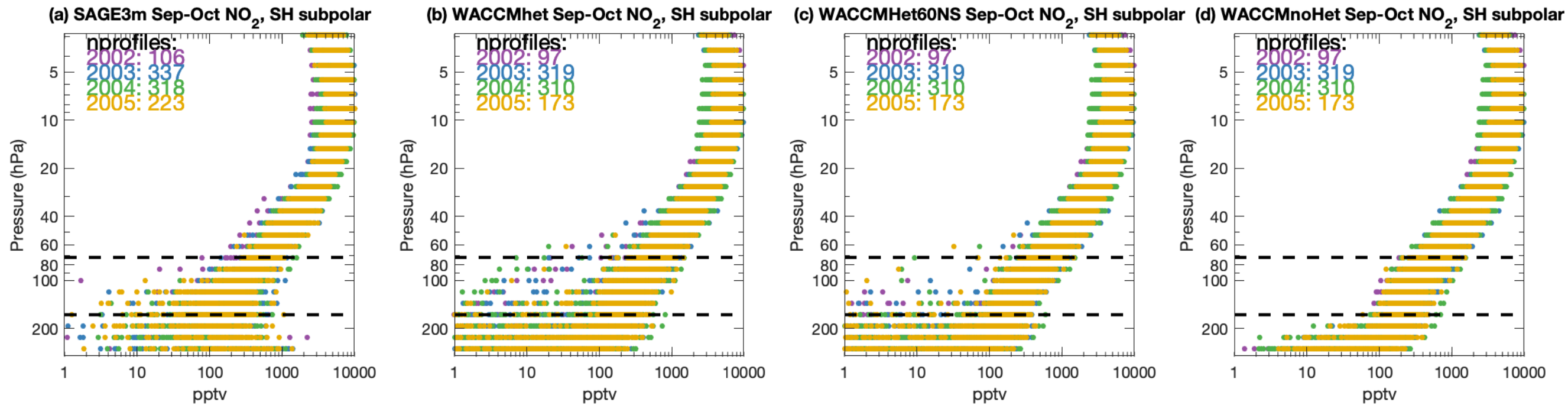
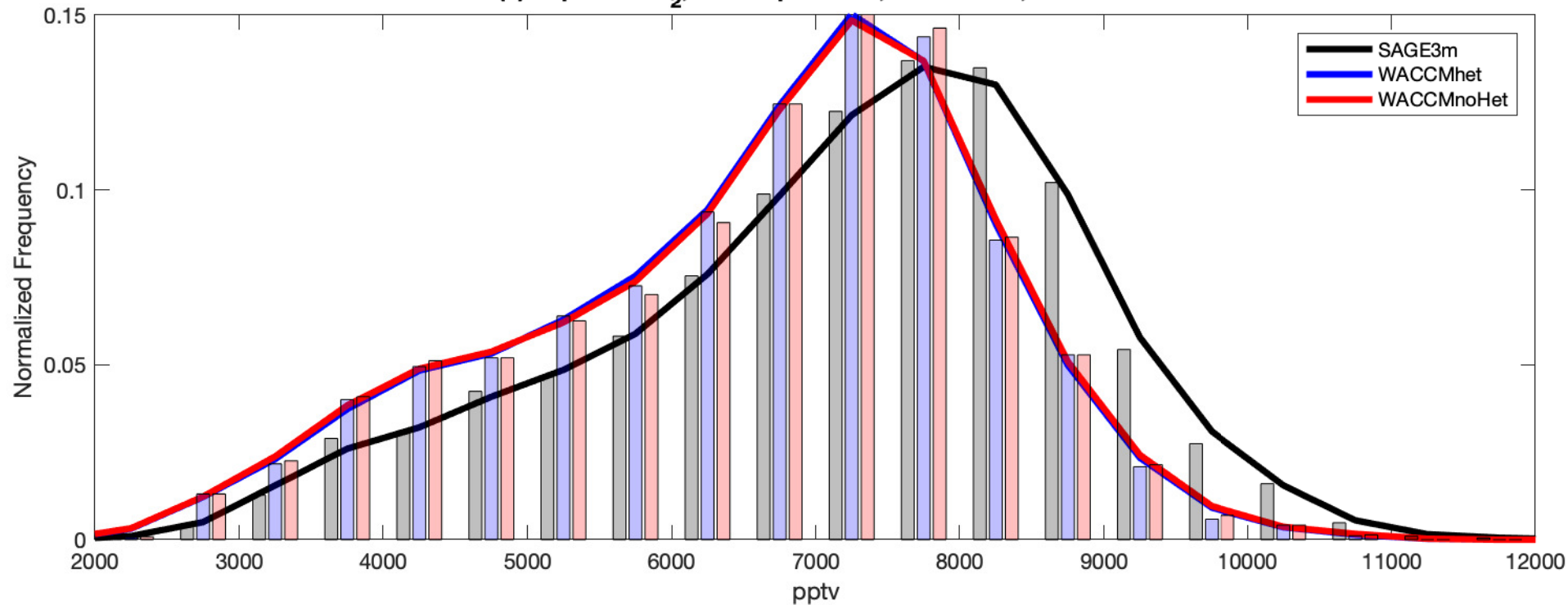


Figure 3.

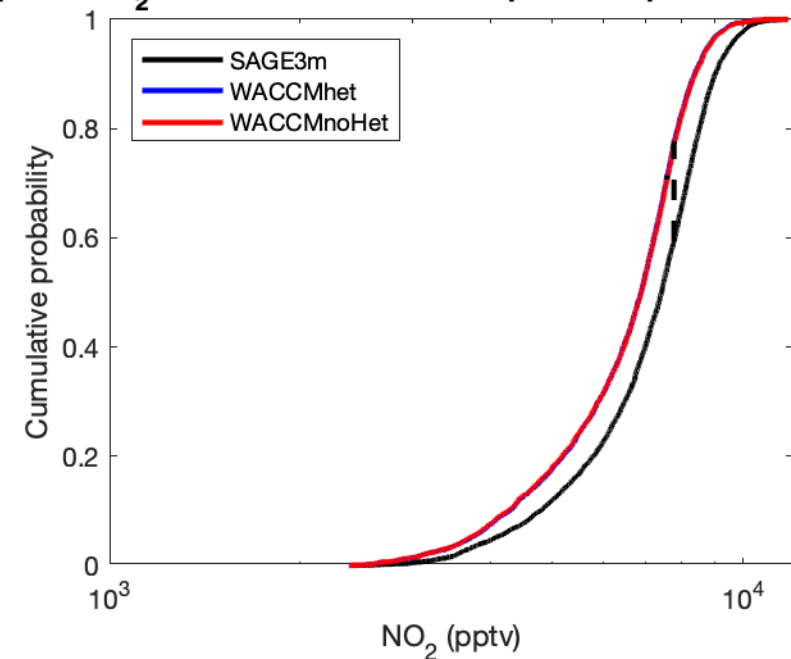


**Figure 4.**

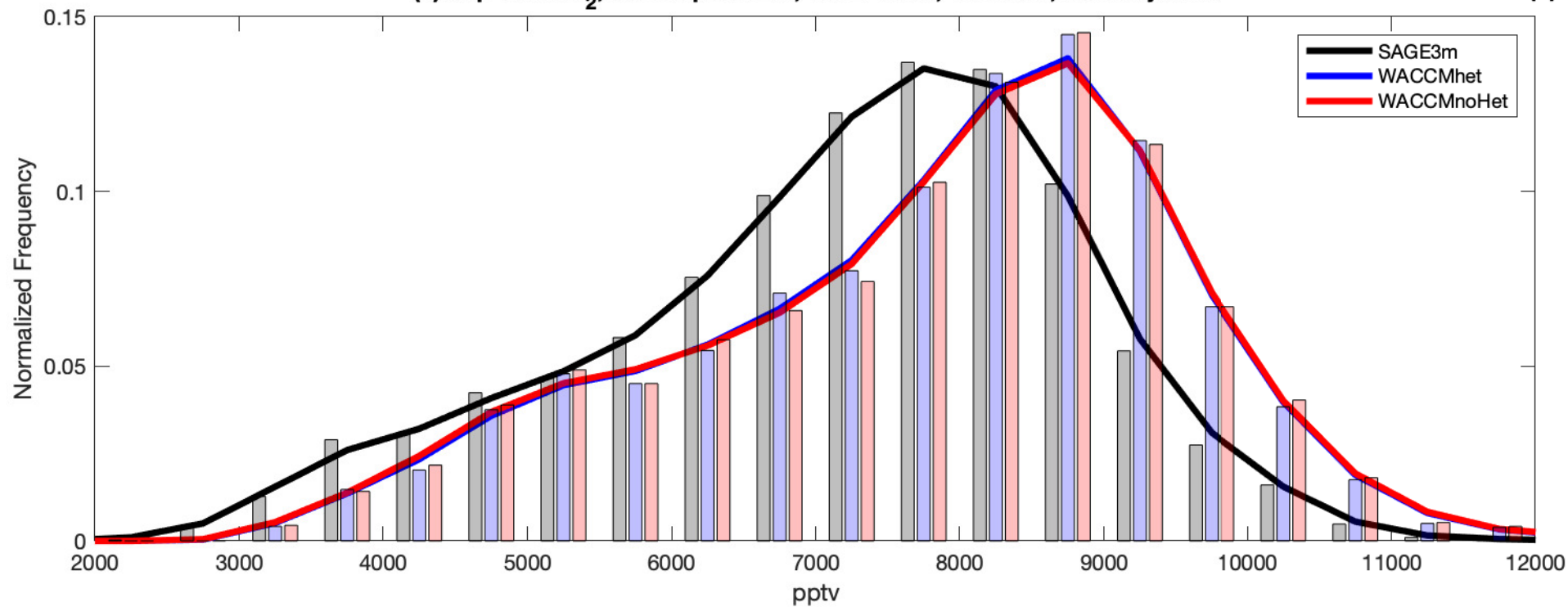
(a) Sep-Oct  $\text{NO}_2$ , SH subpolar Lat, 180E-180W, 11-5 hPa



(b) Empirical  $\text{NO}_2$  distribution functions: Sep-Oct subpolar retrievals, 11-5 hPa



(c) Sep-Oct  $\text{NO}_2$ , SH subpolar Lat, 180E-180W, 11-5 hPa, bias-adjusted



(d) Bias-adjusted empirical  $\text{NO}_2$  distribution functions: Sep-Oct subpolar retrievals, 11-5 hPa

